

# Optimizing Mesh to Improve the Triangular Expansion Algorithm for Computing Visibility Regions

Jan Mikula<sup>1,2\*</sup> and Miroslav Kulich<sup>2</sup>

<sup>1</sup>Department of Cybernetics, Faculty of Electrical Engineering,  
Czech Technical University in Prague, Karlovo náměstí 13,  
Praha 2, 12000, Czech Republic.

<sup>2</sup>Czech Institute of Informatics, Robotics and Cybernetics, Czech  
Technical University in Prague, Jugoslávských partyzánů 1580/3,  
Praha 6, Dejvice, 16000, Czech Republic.

\*Corresponding author(s). E-mail(s): [jan.mikula@cvut.cz](mailto:jan.mikula@cvut.cz);  
Contributing authors: [miroslav.kulich@cvut.cz](mailto:miroslav.kulich@cvut.cz);

## Abstract

This paper addresses the problem of improving the query performance of the *triangular expansion algorithm* (TEA) for computing *visibility regions* by finding the most advantageous instance of the *triangular mesh*, the preprocessing structure. The TEA recursively traverses the mesh while keeping track of the visible region—the set of all points visible from a query point in a polygonal world. We show that the measured query time is approximately proportional to the number of triangle edge expansions during the mesh traversal. We propose a new type of triangular mesh that minimizes the expected number of expansions assuming the query points are drawn from a known probability distribution. We design a heuristic method to approximate the mesh and evaluate the approach on many challenging instances that resemble real-world environments. The proposed mesh improves the mean query times by 12-16% compared to the reference *constrained Delaunay triangulation*. The approach is suitable to boost offline applications that require computing millions of queries without addressing the preprocessing time. The implementation is publicly available to replicate our experiments and serve the community.

**Keywords:** Visibility Region, Triangular Expansion Algorithm, Minimum Weight Triangulation, Navigation Mesh

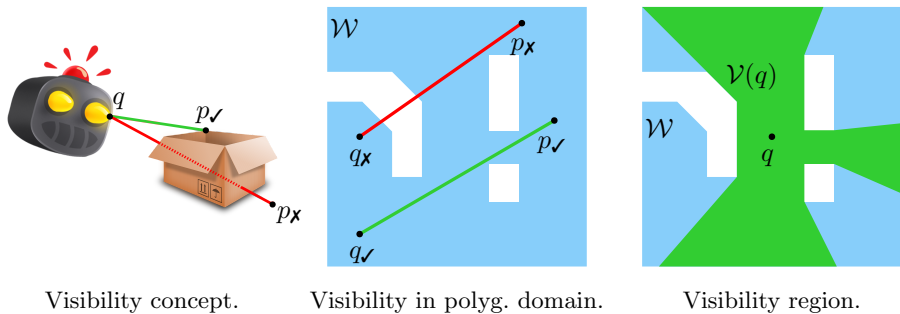


Fig. 1: Visibility and visibility region.

## 1 Introduction

Imagine a mobile robot with omnidirectional vision is provided with a floor map of the building it is in and given the task of finding a specific object with an unknown location somewhere on that floor. In order to be efficient, the robot must first plan a search path that optimizes for the earliest finding of the object and then follow that path. While constructing the search plan, the robot must be able to simulate its own vision at different locations in the map to ensure that particular significant areas and, eventually, the entirety of the map are covered. One way to implement the robot's vision in a known map is by using *computational geometry* and the notion of *visibility*.

Visibility is a general concept to determine if an agent at known configuration  $q$  in world  $\mathcal{W}$  can see certain point  $p$  of the world or if obstacles block its view. In *polygonal domain*<sup>1</sup>, two points  $q, p \in \mathcal{W}$  are visible to each other if segment  $\overline{qp} \subset \mathcal{W}$ . In other words, the segment must be inside the polygon and must not properly intersect<sup>2</sup> the polygon's boundary anywhere (including the holes). In the case of the robot vision simulation, we need to go further and determine all points visible from  $q$ , which form a connected subset of  $\mathcal{W}$  that is known as the *visibility region* [1],  $\mathcal{V}(q)$ , formally defined as

$$\mathcal{V}(q) = \{v \in \mathbb{R}^2 \mid (\forall v)[\overline{vq} \subset \mathcal{W}]\}. \quad (1)$$

Visibility regions take the form of star-shaped polygons that may have attached one-dimensional antennae, which are created when the observer is in line with two of the world's vertices, each blocking the view from the opposite side. In practical use, the antennae are usually neglected; therefore, visibility regions are often regarded as simple polygons and called *visibility polygons* accordingly. See the illustrations of all the basic terms in Fig. 1.

A single visibility region can be computed by the *rotational sweep algorithm* (RSA) [2] in  $\mathcal{O}(n \log n)$  time, where  $n$  is the number of  $\mathcal{W}$ 's vertices.

<sup>1</sup> $\mathcal{W} \subset \mathbb{R}^2$  is a polygon with holes that represents the interior of the map. The outer boundaries and holes of  $\mathcal{W}$  represent the obstacles that impose the motion and visibility constraints.

<sup>2</sup>The segment is allowed to touch the boundary but not cross it to the outside of  $\mathcal{W}$ .

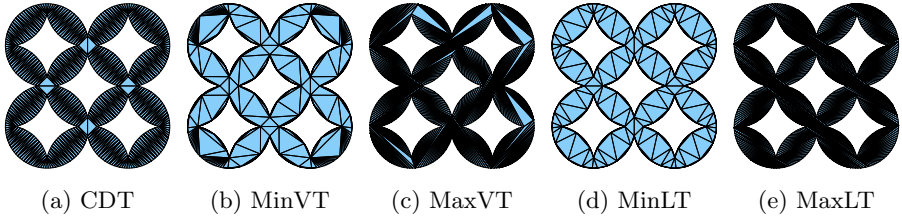


**Fig. 2:** Different triangular meshes of the same map (taken from [4]).

However, in practice, the RSA is outstod by the *triangular expansion algorithm* (TEA) [3], which runs in  $\mathcal{O}(n^2)$  in the worst case but performs much better in practical scenarios. TEA’s authors show that their algorithm is two orders of magnitude faster than the RSA in worlds like a cathedral or country boundary interior and that the worst-case time manifests only at a carefully constructed instance dissimilar to any real-world environment.

The TEA’s idea is simple. As *preprocessing*, triangular mesh  $\mathcal{T}$  is constructed to represent the polygonal world  $\mathcal{W}$ . The mesh is a collection of non-overlapping triangles whose vertices are always some of the  $\mathcal{W}$ ’s vertices and whose union is equal to  $\mathcal{W}$ . The subsequent process of computing visibility regions for any number of input query points, the so-called *query phase*, then utilizes only  $\mathcal{T}$ . TEA’s answer to query  $q$  is initiated by locating triangle  $\Delta_q \ni q$ . Starting from  $\Delta_q$ , the neighboring triangles are recursively traversed while keeping track of the visibility region. TEA’s first highlight is that it only traverses triangles visible from the query point. Thus, in some sense, it is output-sensitive, but not strictly because it may traverse some triangles that do not contribute to the boundary of the result [3]. TEA’s second highlight is that the operations used when traversing the mesh are extremely simple, essentially reducing to answering two orientation predicates per triangle traversal and computing at most two ray-segment intersections when a boundary edge is encountered.

TEA’s authors construct the triangular mesh by the *constrained Delaunay triangulation* (CDT) [5], probably because of its simplicity, fast run time, or good availability of the implementation. But is it the best choice? Does the mesh choice influence the query performance of the algorithm? If yes, is there an optimal mesh, and how the CDT stands compared to the other possible meshes? Interestingly, TEA’s authors do not address any of these questions in [3]. Our previous paper [4], on the other hand, attempts to answer them. We show that when different triangular meshes are used (see Fig. 2 for the examples), the computational time required to answer the same queries on the same map may significantly differ. In order to properly evaluate and compare the meshes, we introduce the notion of the expected number of triangle edge expansions  $\eta_{\mathcal{T}}$ , which strongly relates to the mean query performance of the algorithm  $\bar{t}_q$ . We propose a new type of mesh called MinVT, which approximately minimizes  $\eta_{\mathcal{T}}$  in polygons with holes, and design a heuristic method to

4 *Optimizing Mesh to Improve the TEA*

construct it. Finally, we experimentally evaluate the CDT, MinVT, and other triangular mesh types in terms of  $\eta_{\mathcal{T}}$  and  $\bar{t}_q$  and show that MinVT indeed leads to the best metric values.

This paper is an extension of [4]. Here, we revise the ideas behind MinVT. We newly evaluate some of the assumptions we had when inventing the optimal mesh. We also newly address the preprocessing time, i.e., the time needed to construct MinVT, and optimize it. Furthermore, this paper significantly extends the evaluation part, which is now done on a different, much larger and more challenging world instances from [6]. Overall, this paper is a comprehensive analysis of the topic, while in comparison, the original paper can be seen as the topic's introduction.

The joint contributions of [4] and this paper are the following.

1. We propose a new type of triangular mesh that minimizes the expected number of expansions performed by the TEA. We argue why it should improve the algorithm's mean query time, mathematically formalize the idea, propose a heuristic algorithm to construct the mesh, transparently tune the algorithm's parameters, and experimentally evaluate the approach. The evaluation shows that the closest approximation of the proposed mesh indeed provides the best mean query performance of the TEA compared to numerous other meshes, including the CDT.
2. We propose a simple modification of the TEA called d-TEA to cope efficiently with a more realistic model of visibility that considers limited visibility range  $d$ . Since the d-TEA expands a different number of edges than the TEA, we adapt the proposed mesh to consider this modification. The evaluation shows that the adapted proposed mesh consistently provides the lowest mean number of expansions. However, oddly, for small values of  $d$ , the CDT performs the best in terms of mean query time instead. We provide a possible explanation together with a direction for future investigation.
3. We provide a simple, robust, and efficient open-source implementation of the TEA and the proposed algorithms and the data and scripts used to run our experiments such that our research is easily replicable. The implementation is a robust, versatile, and easy-to-use library that can also serve the scientific community's needs.

The rest of this paper is organized as follows. Sec. 2 reviews the related work with a subsection dedicated solely to the TEA (2.1). Sec. 3 provides a general mathematical formalization of the optimal mesh (3.1) and then works in two simplifying assumptions (3.2). Sec. 4 delivers the algorithms to construct the proposed mesh (4.1-4.2), introduces the d-TEA adaptation (4.3) and details the implementation (4.4). Sec. 5 evaluates our assumptions (5.1), tunes our algorithms (5.2), and presents the final evaluation results (5.3-5.4). Section 6 concludes the paper. And finally, Appx. A provides some additional information about the benchmark instances.

## 2 Related Work

Computing visibility regions has been of high interest in computational geometry since 1979 [1]. Joe and Simpson [7] first provided a correct  $\mathcal{O}(n)$ -time solution for computing visibility regions in simple polygons. Heffernan and Mitchell [8] later proposed the optimal  $\mathcal{O}(n + h \log h)$ -time algorithm for polygon with holes, where  $h$  is the number of holes, improving over the previously best  $\mathcal{O}(n \log n)$ -time RSA by Asano [2]. In the following decades many algorithms for a polygon with holes were published that provide tradeoffs between the preprocessing time and query time, e.g.: Zarei and Ghodsi [9] with  $\mathcal{O}(n^3 \log n)$  preprocessing and  $\mathcal{O}(K + \min(h, K) \log n)$  query time; Inkulu and Kapoor [10] with  $\mathcal{O}(n^2 \log n)$  preprocessing and  $\mathcal{O}(K \log^2 n)$  query time; and Chen and Wang [11] with  $\mathcal{O}(n^2 \log n)$  preprocessing and  $\mathcal{O}(K + \log^2 n + h \log(n/h))$  query time.

The so far mentioned research is theoretical in nature, and most of the published algorithms are quite complex to be practically implemented. In contrast, our background is the autonomous planning of long-time horizon missions for mobile robots, where we utilize visibility regions in complex real-world environments [12–14]. In our field, visibility regions are useful when one needs to guard an art gallery with a set of static observers [15], establish a security guard’s route from which the whole boundary of an area is visible [16], or provide a guarantee that a room is free of intruders [17]. In our recent work [18], we consider a circular robot with radius  $r$  equipped with an omnidirectional sensor with limited visibility range  $d$ . The problem is to plan the shortest route from which the robot can visually inspect the whole environment. We address this NP-hard problem with a heuristic algorithm that utilizes the computation of visibility regions. The regions must be computed for large numbers of query points in order of millions for the most challenging problem instances.

In applications mentioned above, the implementation availability and the actual measured computational time on relevant problem instances are more important than the theoretical properties of the algorithms. Bungiu et al. [3] implement Joe and Simpson’s algorithm for simple polygons [7], and Asano’s RSA for polygons with holes [2] for the CGAL [19] visibility package. In addition to the existing algorithms, Bungiu et al. propose and straightforwardly implement the TEA. As mentioned in the introduction, the authors then show that the TEA is by two orders of magnitude faster than the RSA in real-world scenarios. From the practical point of view, this makes TEA the state-of-the-art algorithm for computing visibility regions.

Motivated by our practically oriented research, an idea to improve the TEA by optimizing its triangular mesh was born. Our previous paper [4] asks the relevant questions on the subject and partially answers them. This paper extends the topic to an in-depth study, as explained in the introduction. Subsec. 2.1 reviews the TEA as proposed by the authors [3].

Furthermore, we want to note that parallel improvement ideas exist that our current work does not address. This paper focuses on the TEA and the class of triangular meshes and finds ways for improvement within the class.

The parallel idea is to consider more general class of meshes, such as convex polygonal ones called *navigation meshes* in the pathfinding literature. Pathfinding, the task of finding the shortest obstacle-free path between two query points in a known map, is closely related to the visibility problems in the polygonal domain [20]. The state-of-the-art geometric pathfinding algorithm Polyanya [21], which runs on convex polygonal meshes, was even adapted in [22] to compute all map vertices visible from another map vertex. We want to emphasize that the two presented ideas are not necessarily competing but can complement each other. In other words, the same considerations that led us to create the MinVT for the TEA might also lead to constructing a polygonal version of the optimized mesh for algorithms like Polyanya [21]. A triangular mesh can be transformed into a convex polygonal mesh by merging some of its triangles into convex polygons. However, some necessary adaptations might not be trivial, like modifying the dynamic programming approach we later describe in Alg. 2 for the general navigation meshes. Hence, the study of such a range is out of the scope of this single paper.

## 2.1 Triangular Expansion Algorithm

Here we revise the TEA proposed in [3], assuming triangular mesh  $\mathcal{T}$  and query point  $q$  is given. The mesh holds information about neighboring triangles, their edges, and vertices.

The algorithm starts by locating triangle  $\Delta_q$ ,  $\Delta_q \in \mathcal{T}$  and  $q \in \Delta_q$ . This can be done by a simple walk in  $\mathcal{O}(n)$ , as the authors suggest. When  $\Delta_q$  is located, a recursive expansion procedure is then called for every one of its edges. The procedure expands through the current edge to the neighboring triangle while restricting the view of  $q$  in between the edge's endpoints. Inside the new triangle, the two non-expanded edges are candidates for the next call of the recursion only if they intersect the current  $q$ 's view. The recursion is called again for any of those edges that also neighbor another triangle. Otherwise, the edge is a *boundary edge*, the current  $q$ 's view is lastly restricted in between its endpoints and stored, and the recursion does not split further from there. By convention, we do not consider the boundary edges to be expanded, despite the view reaches them. After no more expansions can be made, the resulting  $\mathcal{V}(q)$  is the union of all the restricted views formed around  $q$ . See the illustrations of how the TEA works in Fig. 3.

An efficient TEA implementation takes advantage of preordering all the neighbor information in either cw or ccw order. The expansions then rotate around  $q$  while following the same order, and the union of the restricted views is formed naturally. According to the authors' analysis, the worst-case query time is  $\mathcal{O}(n^2)$  because the recursion may split into two views  $\mathcal{O}(n)$  times, and each view may reach  $\mathcal{O}(n)$  triangles. However, splits into two views that reach the same triangle independently may occur only at holes of  $\mathcal{W}$ . This implies that the worst-case query time is rather  $\mathcal{O}(nh)$ , where  $h$  is the number of holes [3].

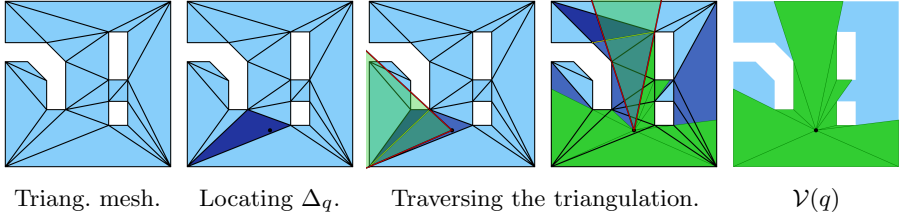


**Fig. 3:** The Triangular Expansion Algorithm.

### 3 Problem Statement

We have learned from TEA’s authors that the algorithm only expands triangle edges that are visible from the query point and neighbor two triangles. These facts are revised in Sec. 2.1. Note that edges that neighbor only one triangle are part of  $\mathcal{W}$ ’s boundary and must be part of any valid mesh. Therefore, the optimal mesh must have the remaining edges organized to be somehow the least visible from a randomly chosen query point. This is the basic idea of our approach. The rest of this section is dedicated to formalizing the idea.

#### 3.1 Optimal Mesh Formalization

We start by defining our quality metrics  $t_q$  and  $\eta_q$ . Assuming  $\mathcal{T}$  and  $q$  are given:  $t_q$  is the computational time to get  $\mathcal{V}(q)$  by the TEA, and  $\eta_q$  is the number of edge expansions recorded in the same scenario. Time  $t_q$  is a value we can measure and wish to minimize, but it is influenced by hidden variables like implementation, hardware setup, state of memory, other processes running, and so on. Number of expansions  $\eta_q$ , on the other hand, is a value that depends only on  $\mathcal{T}$  and  $q$ . Since the number of basic operations done by the TEA scales linearly with the number of expansions, we can expect that  $t_q$  will be proportional to  $\eta_q$ . We use this as an assumption and build our approach upon minimizing  $\eta_q$  (its expected value, to be precise), although we use both metrics to evaluate our approach at the end.

We have established  $\eta_q$  as the definite quality metric for pair  $(q, \mathcal{T})$ . But to define the optimal mesh, we need a metric that is independent of any specific query point. To achieve this, we let the query point be described by random variable  $Q$  with a known two-dimensional *probability density function* (PDF)  $f_{X,Y}$  defined inside polygonal world  $\mathcal{W}$ . Then, the expected number of expansions given triangular mesh  $\mathcal{T}$  is defined as

$$\eta_{\mathcal{T}}(\mathcal{T}) = \mathbb{E}[\eta_q(Q, \mathcal{T})] = \iint_{\mathcal{W}} \eta_q((x, y), \mathcal{T}) \cdot f_{X,Y}(x, y) \, dx \, dy. \quad (2)$$

Now we need to formally define  $\eta_q$ . We have already mentioned one way to compute it: initialize the TEA with  $\mathcal{T}$  and compute  $\mathcal{V}(q)$  while counting the number of expansions in the process. Note that this can be expressed in terms

8 *Optimizing Mesh to Improve the TEA*

of how many times an edge is expanded:

$$\eta_q(q, \mathcal{T}) = \sum_{e \in E(\mathcal{T})} \eta_e(e, q), \quad (3)$$

where  $E(\mathcal{T})$  is the set of all  $\mathcal{T}$ 's edges, and  $\eta_e(e, q)$  is the count of how many independent views of the TEA recursive expansion procedure reach  $e$  from  $q$ . For every view reaching  $e$  from  $q$ , there must be a unique segment on  $e$  whose all points are visible from  $q$ . We can enumerate the endpoints of all such segments using the set-builder notation:

$$\mathcal{S}(e, q) = \{(u, v) \in \mathbb{R}^2 \times \mathbb{R}^2 \mid \overline{uv} \subset e \text{ and } (\forall p \in \overline{uv})[\overline{qp} \subset \mathcal{W}]\}. \quad (4)$$

The expansion count  $\eta_e$  can now be expressed using the cardinality of this set:

$$\eta_e(e, q) = \begin{cases} 0 & \text{if } e \subset \partial\mathcal{W}, \\ |\mathcal{S}(e, q)| & \text{else,} \end{cases} \quad (5)$$

where  $\partial\mathcal{W}$  is the boundary of  $\mathcal{W}$ . The upper case of (5) is to avoid counting the boundary edges, which are, by convention, considered as not expanded even if the view reaches them, as stated in Sec. 2.1. Substituting (5) into (3) and the result into (2), and using the sum rule of integration, we get

$$\begin{aligned} \eta_{\mathcal{T}}(\mathcal{T}) &= \sum_{e \in E_{cand}(\mathcal{T})} \iint_{\mathcal{W}} |\mathcal{S}(e, (x, y))| \cdot f_{X,Y}(x, y) \, dx \, dy, \\ E_{cand}(\mathcal{T}) &= \{e \in E(\mathcal{T}) \mid e \not\subset \partial\mathcal{W}\}. \end{aligned} \quad (6)$$

Finally, let  $\mathcal{T}_{\mathcal{W}}(\mathcal{W})$  be the set of all triangular meshes that represent polygon with holes  $\mathcal{W}$ , then the optimal mesh is

$$\mathcal{T}^* = \arg \min_{\mathcal{T} \in \mathcal{T}_{\mathcal{W}}(\mathcal{W})} \eta_{\mathcal{T}}(\mathcal{T}). \quad (7)$$

The formalization is done. Eq. (4), (6), and (7) describe the optimal triangular mesh for the TEA with pure mathematical notation without the notion of the algorithm itself. Recall the following two assumptions: the number of expansions is proportional to the actual query time performance of the algorithm, and the query points' PDF is known.

### 3.2 Simplifying Assumptions

Although the formalism we introduced precisely describes what we want to achieve, it does not provide any practical way of constructing and evaluating the optimal mesh. For that, we need to introduce two simplifying assumptions:



1. In many applications, we do not know anything about the probability distribution of a certain random variable. In such a case, it is often useful to assume that all possible values are equally likely. This assumption is well known as the *principle of indifference* [23] in the literature. *Applied on the query points implies modeling them using a uniform PDF defined inside  $\mathcal{W}$ .* We use this assumption both in constructing  $\mathcal{T}^*$  and the evaluation, where we draw query points from a uniform distribution using a pseudo-random generator.
2. The second assumption can be expressed simply: *No edge is expanded more than once.* This means that  $\mathcal{W}$  must be a simple polygon or have the property that it is impossible to have multiple independent views from one query point reach the same triangle edge. In our formal language, the assumption can be written as:

$$\mathcal{W} \in \left\{ \mathcal{W}' \mid (\forall q \in \mathcal{W}') (\forall \mathcal{T} \in \mathcal{T}_{\mathcal{W}}(\mathcal{W}')) (\forall e \in E(\mathcal{T})) [|\mathcal{S}(e, q)| \leq 1] \right\}. \quad (8)$$

We use it only when constructing the mesh but do not enforce it in its evaluation. This is the first step away from the exact solution towards a heuristic one. We denote  $\mathcal{T}^*$  as  $\mathcal{T}^{h*}$  and  $\eta$  as  $\eta^h$  to emphasize that the assumption was used.

Now we work these assumptions into the equations from the previous section. Assumption 2 implies that the number of expansions is the same as the number of expanded edges since no edge can be expanded more than once. An edge is expanded if it is at least partially visible from  $q$ ; therefore, Eq. (3) simplifies to

$$\begin{aligned} \eta_q^h(q, \mathcal{T}) &= \sum_{e \in E_{cand}(\mathcal{T})} IsVisible(e, q), \\ IsVisible(e, q) &= \begin{cases} 1 & \text{if } (\exists p \in e) [\overline{qp} \subset \mathcal{W}], \\ 0 & \text{else.} \end{cases} \end{aligned} \quad (9)$$

The new form of (6) is the following:

$$\eta_{\mathcal{T}}^h(\mathcal{T}) = \sum_{e \in E_{cand}(\mathcal{T})} \iint_{\mathcal{W}} IsVisible(e, (x, y)) \cdot f_{X,Y}(x, y) \, dx \, dy. \quad (10)$$

Applying uniform PDF based on Assumption 1 results in

$$\eta_{\mathcal{T}}^h(\mathcal{T}) = \sum_{e \in E_{cand}(\mathcal{T})} \frac{Area(\mathcal{V}_e(e))}{Area(\mathcal{W})}, \quad (11)$$

where  $\mathcal{V}_e$  is the region visible from a segment (see Fig. 4 for the examples):

$$\mathcal{V}_e(e) = \{v \in \mathbb{R}^2 \mid (\exists p \in e) [\overline{vp} \subset \mathcal{W}]\}. \quad (12)$$



**Fig. 4:** Examples of regions  $\mathcal{V}_e(e)$  (green) visible from segments  $e$  (black).

Substituting (11) to (7) and removing constant factor  $1/\text{Area}(\mathcal{W})$ , we get

$$\mathcal{T}^{h*} = \arg \min_{\mathcal{T} \in \mathcal{T}_{\mathcal{W}}(\mathcal{W})} \left[ \sum_{e \in E_{\text{cand}}(\mathcal{T})} \text{Area}(\mathcal{V}_e(e)) \right]. \quad (13)$$

We call the resulting mesh  $\mathcal{T}^{h*}$  *minimum visibility triangulation* or MinVT.

---

**Algorithm 1** MWT for polygon with holes  $\mathcal{W}$  with weights  $w$ .

---

**Ensure:** Weight  $w_{i,j}$  is precomputed for each pair  $(v_i, v_j)$  of  $\mathcal{W}$ 's vertices.

If  $v_i, v_j$  are not visible to each other, then it must be that  $w_{i,j} = \infty$ .

```

1: procedure MINWEIGHTTRIANGULATION( $\mathcal{W}, w, n_{\mathcal{P}}, it_{max}, t_{max}$ )
2:    $\mathcal{T} \leftarrow \text{CONSTRAINEDDELAUNAYTRIANGULATION}(\mathcal{W})$ 
3:   for  $it \leftarrow 1, \dots, it_{max}$  do
4:      $\mathcal{P} \leftarrow \emptyset$  ▷ simple polygon (to be constructed)
5:      $\mathcal{T}' \leftarrow \mathcal{T}$  ▷ mesh with unadded triangles
6:      $\Lambda \leftarrow \{\text{random triangle} \in \mathcal{T}'\}$  ▷ set of candidate triangles
7:     while  $\Lambda \neq \emptyset$  and  $|\mathcal{P}| \leq n_{\mathcal{P}}$  do ▷  $|\mathcal{P}| \sim$  the num. of  $\mathcal{P}$ 's vertices
8:        $\Delta \leftarrow \text{random triangle} \in \Lambda$ .
9:        $\mathcal{P} \leftarrow \mathcal{P} \cup \Delta$ 
10:       $\mathcal{T}' \leftarrow \mathcal{T}' \setminus \Delta$ 
11:       $\Lambda \leftarrow \{\Delta' \in \mathcal{T}' \mid \mathcal{P} \text{ and } \Delta' \text{ share a single edge exclusively}\}$ 
12:    end while
13:     $w_{\mathcal{P}} \leftarrow \text{Reindex weights } w \text{ according to } \mathcal{P}'\text{'s vertices.}$ 
14:     $\mathcal{T}_{\mathcal{P}} \leftarrow \text{MINWEIGHTTRIANGULATIONSIMPLE}(\mathcal{P}, w_{\mathcal{P}})$ 
15:     $\mathcal{T} \leftarrow \mathcal{T}' \cup \mathcal{T}_{\mathcal{P}}$  ▷ merge the new and original meshes
16:    if it elapsed more than  $t_{max}$  sec from the procedure's start then
17:      break
18:    end if
19:  end for
20:  Report  $\mathcal{T}$ .
21: end procedure
```

---

## 4 Solution Approach

### 4.1 Minimum Weight Triangulation

The optimization task in Eq. (13) is, in essence, about finding the *minimum weight triangulation* (MWT) for polygon with holes  $\mathcal{W}$ , where the weights are somehow specifically defined. Finding the MWT for a general set of points on a plane and arbitrarily defined weights is an NP-hard problem [25]. The MWT for a polygon with holes is the constrained version of the MWT for points, similarly as the CDT is the *constrained* version of the *Delaunay triangulation*. The MWT for polygon with holes  $\mathcal{W}$  always contains edges that are part of the  $\mathcal{W}$ 's boundary. Also, we are interested only in triangulating  $\mathcal{W}$ 's interior, not the outside. For computing the MWT for simple polygons, there are known algorithms that are straightforward to implement [24]. However, we found no such convenient algorithm for polygons with holes. Therefore we propose our own heuristic method in Alg. 1.

The method is based on an iterative improvement of the  $\mathcal{W}$ 's CDT with respect to provided weights  $w$ . In each iteration, simple polygon  $\mathcal{P}$  is generated in a randomized fashion by adding triangles from the mesh from the previous iteration (lines 4-12). The simplicity of  $\mathcal{P}$  is assured by adding only triangles that share a single edge with  $\mathcal{P}$  exclusively (line 11). If a triangle shares no edge, more than one edge, or one edge and a vertex other than the edge's endpoints, then the triangle is not considered for addition. This way, no hole can be ever added to  $\mathcal{P}$ . The iteration ends by computing the MWT for  $\mathcal{P}$  with a method from [24] and replacing the triangles added to  $\mathcal{P}$  in the previous iteration mesh with the optimal triangles from MWT, forming the new mesh (lines 13-15). An example of one iteration is shown in Fig. 5.

The MWT for simple polygon  $\mathcal{P}$  is composed of recursive substructure that allows employing *dynamic programming* from [24], shown in Alg. 2. Assuming that  $\mathcal{P}$ 's vertices are numbered in cw or ccw order around its boundary, the method builds tree of weights  $\nu_{i,j}$  associated with subpolygons with vertices between  $p_i$  and  $p_j$  (lines 6-18). The tree is build starting from triangles and is finished when  $\nu_{1,n}$  is determined, since indices  $(1, n)$  correspond to the original polygon. The weights of non-trivial subpolygons defined by indices  $(i, j)$  are determined by evaluating all possible triangles  $\Delta_{i,j,k}$  within them (lines 10-16). Each triangle divides the subpolygon into three parts: the sub-subpolygon

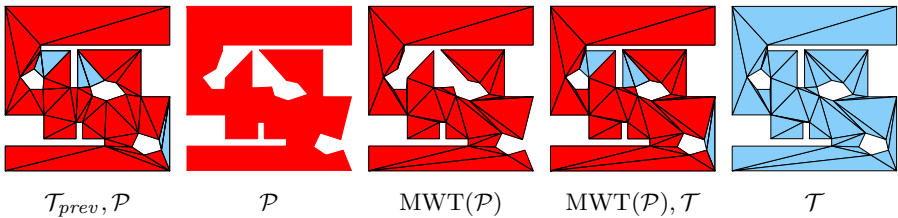


**Fig. 5:** An example of one iteration of the MWT for a polygon with holes.

to the left, the triangle itself, and the sub-subpolygon to the right (line 11). Weight  $\nu_{i,j}$  is determined as the minimal sum of these parts, while index  $k$  that resulted in the minimal sum is stored in  $\kappa_{i,j}$  (line 14). In the end, the resulting MWT for  $\mathcal{P}$  is reconstructed from the  $\kappa$ -indices. The tree structure of  $\kappa$  is recursively traversed starting from  $(1, n)$  (line 19). In each step, pair  $(i, j)$  determines triangle  $\Delta_{i,j,\kappa_{i,j}}$ , which is reported as part of the resulting mesh (lines 23-24). The reconstruction is then called for  $\Delta_{i,j,\kappa_{i,j}}$ 's edges  $(i, \kappa_{i,j})$  and  $(j, \kappa_{i,j})$  until all triangles are eventually reported (lines 25-26).

The whole framework for constructing MWT for polygon with holes, i.e., Alg. 1-2, has one parameter and two stopping conditions. The parameter is the maximum number of vertices  $n_{\mathcal{P}}$  of simple polygon  $\mathcal{P}$ . If  $\mathcal{P}$  reaches this size,

---

**Algorithm 2** MWT for simple polygon  $\mathcal{P}$  with weights  $w$ . Based on [24].

---

**Ensure:**  $\mathcal{P}$  is simple and its vertices are denoted as  $p_1, \dots, p_n$  consecutively around its boundary. The weight of  $(p_i, p_j)$  is accessed via  $w_{i,j}$ . If  $p_i, p_j$  are not visible to each other, then it must be that  $w_{i,j} = \infty$ .

```

1: procedure MINWEIGHTTRIANGULATIONSIMPLE( $\mathcal{P}, w$ )
2:   for  $i \leftarrow 2, \dots, n$  do
3:      $\nu_{i-1,i} \leftarrow 0$ 
4:      $\kappa_{i-1,i} \leftarrow 0$ 
5:   end for
6:   for  $gap \leftarrow 2, \dots, n-1$  do
7:     for  $i \leftarrow 1, \dots, n-gap$  do
8:        $j \leftarrow i+gap$ 
9:        $\nu_{i,j} \leftarrow \infty$ 
10:      for  $k \leftarrow i+1, \dots, j-1$  do
11:         $\nu_{new} \leftarrow \nu_{i,k} + \frac{1}{2}(w_{i,j} + w_{j,k} + w_{k,i}) + \nu_{k,j}$ 
12:        if  $\nu_{new} < \nu_{i,j}$  then
13:           $\nu_{i,j} \leftarrow \nu_{new}$ 
14:           $\kappa_{i,j} \leftarrow k$ 
15:        end if
16:      end for
17:    end for
18:  end for
19:  RECONSTRUCT( $1, n, \mathcal{P}$ )
20: end procedure
21: procedure RECONSTRUCT( $i, j, \kappa, \mathcal{P}$ )
22:   if  $\kappa_{i,j} \neq 0$  then
23:      $k \leftarrow \kappa_{i,j}$ 
24:     Report triangle  $\Delta_{i,j,k}$ .
25:     RECONSTRUCT( $i, k, \kappa, \mathcal{P}$ )
26:     RECONSTRUCT( $j, k, \kappa, \mathcal{P}$ )
27:   end if
28: end procedure

```

---

its construction is finished prematurely. But setting  $n_{\mathcal{P}} = \infty$  is also valid.  $\mathcal{P}$  is then always maximal such that adding any other unadded triangle would break its simplicity. The stopping conditions are the maximal number of iterations  $it_{max}$  and the maximal computational time  $t_{max}$ , and they are evaluated in the main loop of Alg. 1.

## 4.2 Minimum Visibility Triangulation

The difference between the MWT and MinVT is the definition of weights for every pair of  $\mathcal{W}$ 's vertices  $(v_i, v_j)$ . While the MWT assumes the weights are given, the MinVT includes their exact definition. This subsection primarily concerns how these weights are computed. But first, the following paragraph summarizes some general information about the weights, including the notation used in the rest of this paper.

It is equivalent to say that  $w_{i,j}$  is defined for the pair of  $\mathcal{W}$ 's vertices  $(v_i, v_j)$  as to say that it is defined for the segment  $\overline{v_i v_j}$ . The segment  $\overline{v_i v_j}$  can also be called *edge*  $e_{i,j}$ . For Alg. 1-2 to produce a valid triangular mesh, the following is required of the weights:

$$w_{i,j} = w_{j,i} = \begin{cases} \infty & \text{if } \overline{v_i v_j} \notin \mathcal{W}, \\ 0 & \text{if } \overline{v_i v_j} \subset \partial\mathcal{W}, \\ \text{any finite value} & \text{else.} \end{cases} \quad (14)$$

Note that the weights must be symmetrical. The first case of (14) refers to the *forbidden edges*, which can never appear in any valid triangulation because their endpoints are not visible to each other; therefore, they have infinite weights. The second case concerns the *boundary edges*, which must be present in every valid mesh of  $\mathcal{W}$  and, by convention, they have zero weights. The last case is about *candidate edges* which may be present in a valid triangulation and sometimes must; therefore, their value must be finite. Only the candidate edges are the ones that are optimized and their weight value matters to the optimization result. *Thereinafter, when we speak about a weight of an edge, we implicitly mean the edge is a candidate edge.*

MinVT's weights are defined according to (13) as  $w_{i,j} = \text{Area}(\mathcal{V}_e(e_{i,j}))$ , where  $\mathcal{V}_e(e)$  is the region visible from edge  $e$  defined in Eq. (12). This region is a structure similar to the visibility region from a point, but as if the point traveled along the segment from one endpoint to the other while collecting all points that were visible sometime during that journey. We use an approximate computation that utilizes the classic TEA running on an un-optimized CDT mesh. The computation samples the segment  $e = \overline{uv}$  in between its endpoints equidistantly with points  $S(e, d_{smp}) = \{s_1, s_2, \dots\}$  such that the sampling distance is maximal but not larger than parameter  $d_{smp}$ , unless  $|e| \leq d_{smp}$ . If the latter condition holds, then just one sample in the middle of the edge is used instead, i.e.,  $S(e, d_{smp}) = \{s_1 = (u + v)/2\}$ . The desired region is then

obtained as the union of the visibility regions from all points in  $S$ :

$$\mathcal{V}_e(e) = \bigcup_{s \in S(e, d_{\text{samp}})} \mathcal{V}(s). \quad (15)$$

### 4.3 Limited Visibility Range

Visibility regions can be thought of as a general concept to model an agent's ability to see or cover part of the environment in which it operates. The visibility regions considered so far are the most idealized case of an omnidirectional vision with an unlimited visibility range. However, visibility regions can be subject to additional constraints in real-life applications. For example, in robotics, omnidirectional sensors are common, but their resolution over longer distances is always limited to finite range  $d$ . If we wanted to model this situation, we could run the TEA to get the standard visibility region and then intersect it with a circle. See the example in Fig. 6. The result can be formally defined as

$$\mathcal{V}(q, d) = \{v \in \mathbb{R}^2 \mid (\forall v)[\overline{vq} \subset \mathcal{W} \text{ and } |\overline{vq}| \leq d]\}. \quad (16)$$

However, if the result was considerably smaller than the original, we would have wasted much computational power when TEA expanded beyond range  $d$ .

To be more efficient, we suggest an early exit strategy for the TEA. The only change is that edges that do not intersect the circle of radius  $d$  centered in the query point are handled the same way as boundary edges. We call this modification d-TEA. Note that  $\text{TEA} = \infty\text{-TEA}$ . The output of d-TEA still needs to undergo the intersection with the circle to get  $\mathcal{V}(q, d)$ , but the computational advantage of d-TEA is that it expands only edges that contribute to the final result. The circle intersection can be computed efficiently by rotating around the query point, taking advantage of the region's star shape.

Trivial as it may seem, the extension from TEA to d-TEA changes how many edges are expanded, thus also the optimal mesh, depending on  $d$ . We encourage the reader to incorporate  $d$  into every equation from (2) to (13), but here we state only the final result.

We denote the d-TEA's equivalent to MinVT as d-MinVT, and define its weights as  $w_{i,j} = \text{Area}(\mathcal{V}_e(e_{i,j}, d))$ , where

$$\mathcal{V}_e(e, d) = \{v \in \mathbb{R}^2 \mid (\exists p \in e)[\overline{vp} \subset \mathcal{W} \text{ and } |\overline{vp}| \leq d]\}. \quad (17)$$

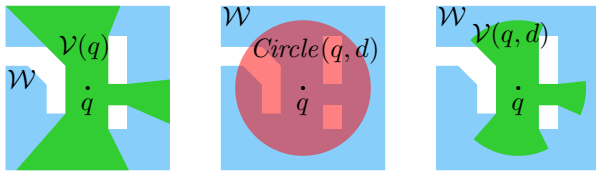


**Fig. 6:** An example of a visibility region with limited range  $d$ .



**Fig. 7:** Examples of regions  $\mathcal{V}_e(e, d)$  visible from segments  $e$  for different  $d$ s.

See Fig. 7 for the examples. To evaluate d-MinVT, we obtain  $\mathcal{V}_e(e, d)$  in the following way. We first compute  $\mathcal{V}'_e(e)$  according to (15) but using d-TEA instead of TEA. Then  $\mathcal{V}'_e(e)$  is intersected with a shape that is the result of a union of the following: two circles with radius  $d$ , each centered at one of  $e$ 's endpoints, and a belt of width  $2d$  going from one endpoint to the other.

#### 4.4 TřiVis: The Implementation

Our C++ implementation of the TEA, d-TEA, MWT, and MinVT, is publicly available<sup>3</sup>, along with the data and scripts to run our experiments. We call the implementation TřiVis<sup>4</sup>. TřiVis is a robust, versatile, easy-to-use, self-contained, open-source C++ library for computing visibility-related structures.

The robustness is ensured using Shewchuck's adaptive robust orientation predicates [26] in the TEA expansion procedure. Besides the TEA for computing visibility regions, it contains TEA variants optimized for determining visibility between two query points and for computing all map's vertices visible from a given point, all with or without considering the limited visibility range.

The visibility regions come with edge and vertex flags, determining their origin. For example, a visibility region's edge can be either part of the map boundary or free space. A vertex can be either a vertex of the map or computed as a ray-segment intersection. This information can be handy if the topological relationship between the region and the map is essential to users.

Thanks to the initial abstract representation of the visibility region, the TEA expansion procedure and computing ray-segment intersections are separated in the implementation. Therefore, users can save run time by skipping computing the intersections if the abstract representation is sufficient for their needs.

Locating the triangle that contains the query point is implemented efficiently. It can be done by a simple walk in  $\mathcal{O}(n)$ , as Bungiu et al. [3] suggest, but we do it with a more sophisticated technique called *bucketing* [27, 28], which uses rectangular regions called *buckets*. The bucket containing  $q$  is identified first by simply rounding the  $q$ 's coordinates and using a lookup table. The bucket points to all triangles in  $\mathcal{T}$  that share a non-zero intersection with it, so  $\Delta_q$  is found checking only these. Bucketing requires another round of

<sup>3</sup><http://imr.ciirc.cvut.cz/Research/TřiVis>

<sup>4</sup>We call the implementation TřiVis in the original conference paper [4]. We renamed it TřiVis because it is the third version, and *tř*i means *three* in Czech. Letter ř is pronounced as "rzh" but with the r rolled.

preprocessing to determine the intersecting triangles for each bucket and generally does not improve the worst-case time  $\mathcal{O}(n)$  to find  $\Delta_q$ <sup>5</sup>. However, in practice, the expected run time is  $\mathcal{O}(1)$  for most meshes when the bucket size is reasonably chosen.

## 5 Experiments, Results, and Discussion

This section describes and discusses all the experiments and results to evaluate our assumptions (5.1), tune our algorithms (5.2) and thoroughly test our approach (5.3-5.4). All these experiments have two things in common: the type of benchmark instances and hardware settings. The benchmark instances are the complex polygonal maps from [6] based on the videogame Iron Harvest from KING Art Games. From the set of 35, we randomly select 10 of them for tuning purposes and use the rest for the final evaluation. Appx. A provides more information about the maps. All the experiments are executed on a personal laptop Legion 5 Pro 16ITH6H with Intel Core i7-11800H (4.60 GHz), 16 GB of RAM, and running Ubuntu 20.04.5 LTS. The implementation is single-threaded.

Additionally, through this section, we often refer to the *relative value* or *percentage gap* of some variable. Both refer to the same definition:

$$\%val = 100 \cdot (val - val_{ref}) / val_{ref}, \quad (18)$$

where  $val$  is the absolute value and  $val_{ref}$  is the reference absolute value of the same type. In all cases, we use the CDT as the reference.

### 5.1 Assumptions Evaluation

This section experimentally shows that the assumptions from Sec. 3 approximately hold. First, we show that the computational time  $t_q$  is approximately proportional to the number of expansions  $\eta_q$  for our experimental setup. Second, we address the relationship between  $\eta_{\mathcal{T}}$  and  $\eta_{\mathcal{T}}^h$  from Eq. (6) and (11), respectively, for a simple polygon and polygon with holes. In both scenarios we use the two mesh instances shown in Fig. 8.

---

<sup>5</sup>This is because a bucket can still intersect  $\mathcal{O}(n)$  triangles in the general case.

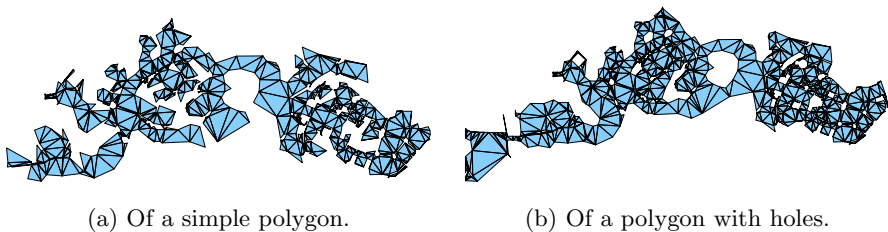


**Fig. 8:** An example of triangular mesh.



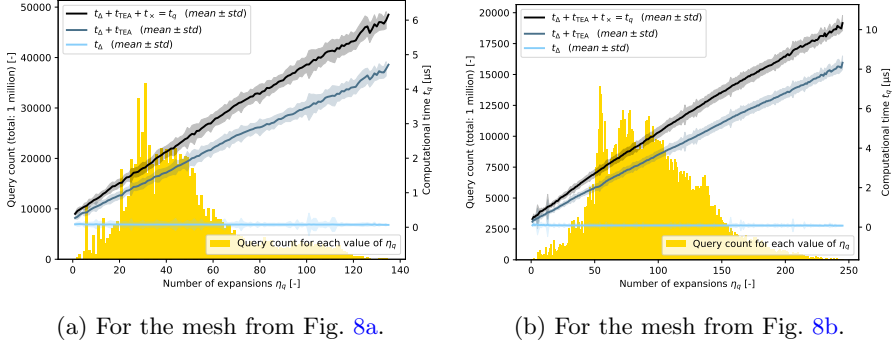


**Fig. 9:** Experimental evaluation of the relation between  $\eta_q$  and  $t_q$ .

### 5.1.1 Relation Between $\eta_q$ and $t_q$

We have run the TEA on two meshes to find visibility regions for one million uniformly random query points, measuring both metrics. For each value of  $\eta_q$ , Fig. 9 shows how many times this value was recorded (gold) and the corresponding mean value  $\pm$  standard deviation of  $t_q$  (black). Our implementation allows to measure  $t_q$  as the sum of three consecutive times:  $t_q = t_\Delta + t_{TEA} + t_\times$ , where  $t_\Delta$  is the time to locate  $\Delta_q$ ,  $t_{TEA}$  is the time of the expansion procedure without computing the ray-segment intersection points between edges and  $q$ 's views, and  $t_\times$  is the time to compute all these intersection points. The figures furthermore show the plots of  $t_\Delta$  (light blue) and  $t_\Delta + t_{TEA}$  (dark blue). We can see that the expansion procedure with time  $t_{TEA}$  is the most computationally demanding part. Time  $t_\Delta$  is constant and very small, while both  $t_{TEA}$  and  $t_\times$  depend almost linearly on the number of expansions. This observation is expected for  $t_{TEA}$ , but it is not obvious for  $t_\times$ , because this part logically depends purely on the output and not on the mesh. A possible explanation is that more expansions usually relate to a more complex output; thus, more intersection points must be computed.

The overall conclusion is that the total time  $t_q$  to compute visibility region is approximately proportional to the number of expansions  $\eta_q$  in the case of our experimental setup. Minimizing  $\eta_q$  to improve  $t_q$  is thus a solid idea.

### 5.1.2 Relation Between $\eta_\tau$ and $\eta_\tau^h$

While  $\eta_\tau$  is the expected number of edge expansions,  $\eta_\tau^h$  is the expected number of expanded edges. The optimal mesh for the TEA wishes to minimize the first, but our heuristic approach minimizes the second with MinVT. The process of deriving  $\eta_\tau^h$  (Sec. 3.2) implies that if the assumption (8) holds for assessed  $\mathcal{W}$ , then  $\eta_\tau = \eta_\tau^h$ . We know that (8) always holds for simple polygons, but it may not hold for polygons with holes. Since none of the practical instances we solve later in the evaluation is simple, we must hope that for them (8) holds approximately. The following experiment addresses these issues.

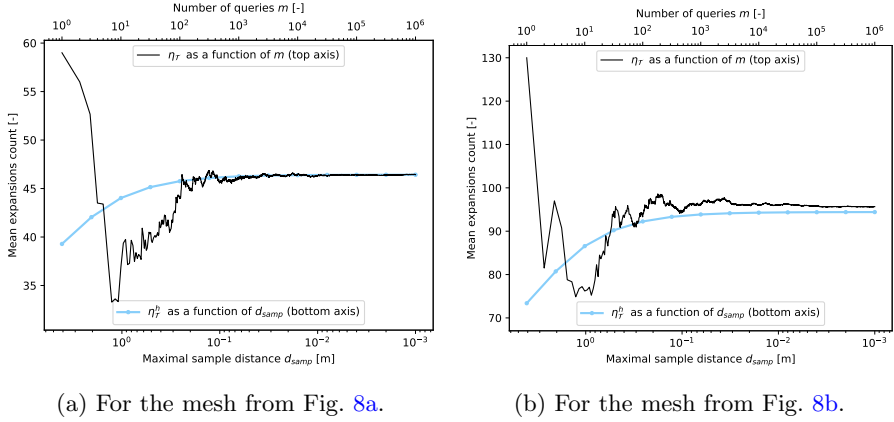


**Fig. 10:** Experimental evaluation of the relation between  $\eta_T$  and  $\eta_T^h$ .

The TEA was run for  $m$  uniformly random query points while recording the numbers of expansions, which were then averaged to get the estimate of  $\eta_T$ . The estimate of  $\eta_T^h$  was obtained according to Eq. (11) and (15) for several values of sampling distance  $d_{samp}$ . Fig. 10 shows  $\eta_T$  (black) as the function of  $m$  (top axis), and  $\eta_T^h$  (light blue) as the function of  $d_{samp}$  (bottom axis). We can see that the two plots converge to the same value in the case of the simple polygon (Fig. 10a), according to our expectations. The final gap of  $\eta_T^h$  from  $\eta_T$  is only  $-0.04\%$ . In the case of the polygon with holes, the two plots also converge to a value, but each to a slightly different one (Fig. 10b). The final gap (of  $-1.3\%$ ) is because some edges were expanded more than once in the evaluation, which is not coped by the value of  $\eta_T^h$ . The gap can be seen as the estimate of how imprecise our approach is when computing the optimization criterion inside a polygon with holes representing a realistic yet complex environment.

## 5.2 Construction Tuning

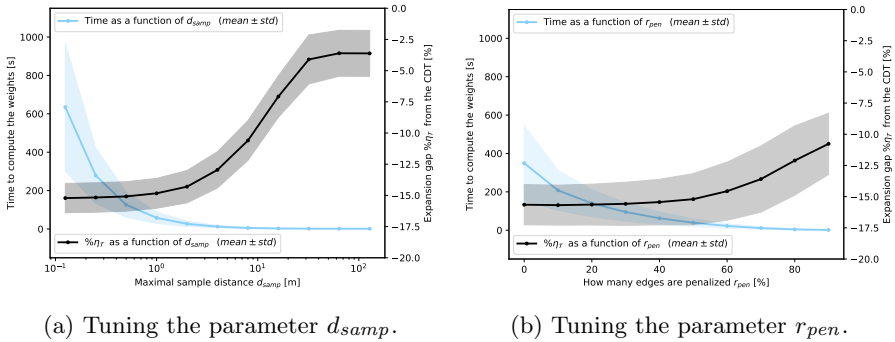
This subsection finds the best compromise between the quality of the MinVT mesh and the computational time required for its construction. The goal is to construct a sufficient quality mesh without wasting precious computational time. Tab. 1 shows all the tunable parameters of the construction procedure that affect both values. It holds that if a specific value improves the quality of the mesh, it slows the construction time down. The rest of this section describes the experiments that lead us to use the specific values, shown in the “Value” column, in the final evaluation. The map instances we use for tuning the parameters differ from those for the final evaluation. Here, we use only the 10 instances marked with ✓ in Tab. A1. For the evaluation in later sections, we use the 25 unmarked instances.

**Table 1:** Tunable parameters of the MinVT construction.

Symbol	Where introduced	Meaning	Value	Unit
$d_{s\text{amp}}$	Sec. 4.2, Eq. (15)	Maximal sampling distance for $\mathcal{V}_e$	$\{2, 4, 8\}$	m
$n_{\mathcal{P}}$	Sec. 4.1, Alg. 1	Maximal size of simple polygon $\mathcal{P}$	450	1
$it_{\text{max}}$	Sec. 4.1, Alg. 1	Maximal number of MWT iterations	200	1
$t_{\text{max}}$	Sec. 4.1, Alg. 1	Maximal run-time of MWT	6	s
$r_{\text{pen}}$	The end of Sec. 5.2	How many edges are penalized	$\{0, 50\}$	%

We start with the maximal sampling distance  $d_{s\text{amp}}$ . A lower value means we get a better estimate of the MinVT weights, but it will take longer to compute them. To rule out the influence of  $\eta_{\mathcal{T}}^h \neq \eta_{\mathcal{T}}$ , we use simple polygon versions of the maps. The simple polygons are generated using the procedure in Alg. 1 with  $n_{\mathcal{P}} = \infty$ . See Fig. 8a for the example of a simple polygon generated from map p11 (Fig. 8b). In the experiments, we use Alg. 2 to get the MinVT mesh for  $d_{s\text{amp}} \in \{.125, .25, .5, 1, 2, 4, 8, 16, 32, 64, 128\}$ . Each is then evaluated on 1 million uniformly random query points and mean number of expansions  $\eta_{\mathcal{T}}$  is recorded. Fig. 11a shows  $\% \eta_{\mathcal{T}}$  (black, right axis) and computational time to compute the weights (light blue, left axis) as the function of  $d_{s\text{amp}}$ .  $\% \eta_{\mathcal{T}}$  is the percentage gap from the CDT that we also evaluated for reference. Both plots are averaged over the maps, and the standard deviation is included in the background as half-transparent. We can see that for  $d_{s\text{amp}} < 1$  the value of  $\% \eta_{\mathcal{T}}$  converges, but the time to get there is enormous. On the other side for  $d_{s\text{amp}} > 10$  we see very fast computations but poor quality. Values between 1 and 10 seem to provide the best compromise. We select  $d_{s\text{amp}} \in \{2, 4, 8\}$ .

Next, we tune the parameters of Alg. 1:  $n_{\mathcal{P}}$ ,  $it_{\text{max}}$ , and  $t_{\text{max}}$ . In the first set of experiments, we use  $n_{\mathcal{P}} \in \{2^x \mid x \in \{2, \dots, 12, \infty\}\}$ ,  $it_{\text{max}} = 10000$ ,  $t_{\text{max}} = 360$ , and  $d_{s\text{amp}} = 2$ . We run Alg. 1 several times with different settings on each map (with holes), and for each iteration, we record the current weight of the mesh and time from the start. The mesh weight as a function of time is shown in Fig. 12. For clarity, we select to show results

**Fig. 11:** Tuning the parameters related to computing weights.

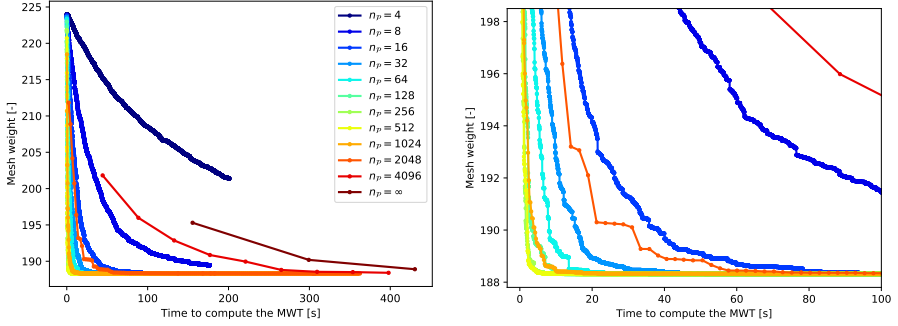


**Fig. 12:** Tuning the MWT. The right figure is a detail of the left one.

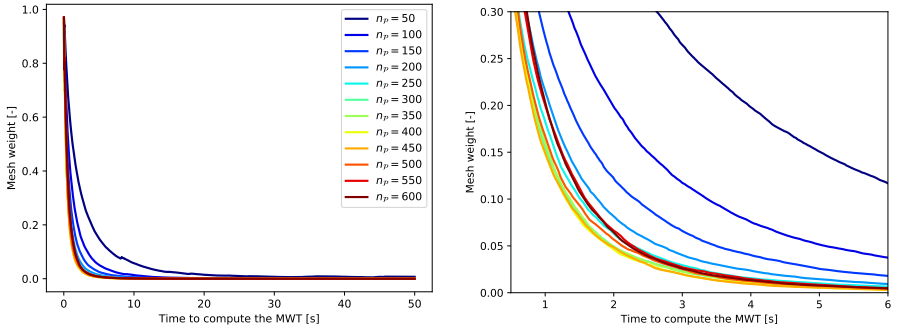


**Fig. 13:** Tuning the MWT; higher resolution. The right figure is a detail.

for just a single map (p14) and we do not show the standard deviation. For  $n_P \in \{16, \dots, 4096\}$ , the weight converges within the chosen iteration and time window. For  $n_P \in \{64, \dots, 1024\}$ , it converges much more quickly compared to the other values. To select the best value, we are improving the resolution to  $n_P \in \{50, 100, 150, \dots, 600\}$  and shrinking the time window to  $t_{max} = 50$ . The corresponding plots are in Fig. 13. This time, we show the average plots over all maps. Based on this second set of experiments, we are selecting  $n_P = 450$  as the best value because, at any given time, it provides the lowest weight and quickly converges. Based on the time and iteration window of the convergence we are selecting  $it_{max} = 200$ , and  $t_{max} = 6$ .

Finally, having  $d_{samp} = 2$ ,  $n_P = 450$ ,  $it_{max} = 200$ , and  $t_{max} = 6$ , we are still looking for a way to improve the time to compute the weights without a dramatic loss of quality. Based on the visual analysis of MinVT meshes, we have noticed that the mesh seldom chooses among the longest of the candidate edges. An idea was born to penalize  $r_{pen}\%$  of the longest candidate edges  $e_{i,j}$  by setting their weight to  $w_{i,j} = 1000 + |e_{i,j}|$ . It saves time because determining the penalized weight is significantly less computationally demanding than the non-penalized weight  $w_{i,j} = Area(\mathcal{V}_e(e_{i,j}))$ . The penalization means that the

$(100 - r_{pen})\%$  of the shortest edges are always preferred over the  $r_{pen}\%$  of the longest edges. If there is no suitable short edge to be selected, then MWT at least optimizes among the long edges according to their length. We run the same set of experiments as when tuning  $d_{samp}$  except the variable parameter is now  $r_{pen}$ , and the maps are with holes. The corresponding plots are shown in Fig. 11b. We select  $r_{pen} = 0$  as the default and  $r_{pen} = 50$  as the best compromise between quality and time.

### 5.3 Mesh Evaluation: TEA

The final evaluation is done on the 25 map instances from [6], which are not marked in Tab. A1, in the following way. First, the mesh under evaluation is constructed to represent the given map. The CDT is constructed using Triangle [29], all the other meshes using the MWT (Alg. 1). The time of construction  $t_c$  is recorded. Then, one million uniformly random query points are generated inside the map using a pseudo-random generator initialized always with the same seed to ensure fair conditions for every mesh. Then, the TEA is run to compute a visibility region for each query point. The number of edge expansions  $\eta_q$  done by the TEA and computational time  $t_q$  are recorded in the process. These values are then averaged to obtain  $\eta_{\mathcal{T}}$  and  $\bar{t}_q$ . We report the metric's absolute values for the CDT, and for other meshes, we report the relative percentage gap from the reference CDT value according to (18).

Besides CDT as the reference, we evaluate a number of MinVT variants, all of which can be enumerated as  $\{', d-\}\text{MinVT}\{', O\}-\{2, 4, 8\}$ . The prefix d- means limited visibility range  $d$  was used when computing the weights. The variant without the prefix means  $d = \infty$ . The O stands for *Optimized*, and it refers to  $r_{pen} = 50$ . No O implies  $r_{pen} = 0$ . The suffix number is the value of  $d_{samp}$ . We also evaluate the *minimum length triangulation* MinLT with weights defined as  $w_{i,j} = |e_{i,j}|$ . Furthermore, we think evaluating the full range of meshes is interesting, not just the good ones and the reference. Therefore, we also include the MaxLT and MaxVT-2, which have negative weights of MinLT and MinVT-2, respectively. We show all eventuated meshes constructed on a unique map<sup>6</sup> in Fig. 2.

The complete results for every test map and mesh type, excluding MinVT with the d- prefix, are shown in Tab. 2. We can see that the CDT performs 177.5 expansions and runs for 8.44  $\mu\text{s}$  per query, on average over all maps. The CDT construction time is effectively zero compared to other meshes. The average MinLT takes 6s to construct and improves the number of expansions and query time by 8% and 12%, respectively. The best mesh in terms of query performance is MinVT-2, improving on CDT by 14% and 16% on average, according to the two respective metrics. This observation is essential because MinVT-2 is the closest approximation of the proposed optimal mesh, thus validating the overall approach.

---

<sup>6</sup>This map was specifically designed to emphasize the differences between the meshes.



Constructing the MinVT-2 takes 212s on average. We can observe, however, that the MinVT construction times greatly depend on parameters  $d_{\text{samp}}$  and  $r_{\text{pen}}$ , which affect how the weights are computed. This observation and the fact that the MWT has a maximal run time limit set to 6s suggest that computing the weights is the main bottleneck. It could be addressed by more efficient computation of the region visible from an edge, for example, with a specialized algorithm based on the TEA that does not require edge sampling. We are halfway through implementing this algorithm, but it could not yet be used in this study due to insufficient robustness. We expect this novel algorithm to better approximate the optimal mesh than the MinVT-2 and approach the MinLT with the construction times. In the current state of affairs, however, it seems that MinVTO-4 provides the best compromise between construction and query times among the MinVT meshes with 13s of construction, and 12/14% average improvement over the CDT.

Lastly, note that using the MaxLT and MaxVT-2 meshes results in the worst query performance by far, according to expectations.

## 5.4 Mesh Evaluation: d-TEA

The previous results in Tab. 3 can be seen as the results for the d-TEA with unlimited visibility range. In this section, we present the d-TEA results for some other, finite, values of  $d$ : 128, 64, 32, 16, 8, 4, and 2.<sup>7</sup> Recall that for finite values, the output region returned by d-TEA is intersected with a circle of radius  $d$  centered in the query point. We note that we measure the computational time of this operation,  $t_o$ , and add it to the total query time  $t_q$ .

The extended results are shown in Tab. 3. We present only the averaged values (over all maps) because we could not fit that many tables in this paper. Note that the whole Tab. 2 is virtually contained in Tab. 3 (see the \*-marked values). Also, be aware that the CDT values are still absolute, while for the other meshes, we present relative values except  $\bar{t}_c$ . They extended results newly include the d-MinVT meshes for the finite values of  $d$ .

We can see that for every mesh, the construction time, number of expansions, and query times are all getting lower with lower values of  $d$  due to the early exit strategy of d-TEA. However, this rule has one exception: the query times for  $d = 128$  are higher than for  $d = \infty$ . The numbers of expansions are relatively similar for these two specific values, but for  $d = 128$ , there is an additional computational burden in resolving the circle intersection. Time  $t_o$  to compute the circle intersection outweighs the time saved by sparing some of the expansions; thus, there is an increase in total query time.

Let us now compare the meshes. We can see that across all finite values of  $d$ , the d-MinVT-2 mesh consistently provides the least number of expansions, while MinVT-2 is often worse than the MinLT. This confirms that the optimal mesh, as we defined it, is not generally the same for the d-TEA as for the TEA.

---

<sup>7</sup>Recall that we measure  $d$  in meters, which is arbitrary in essence. The important thing is that we measure it in the same unit as the maps and parameters like  $d_{\text{samp}}$ . The reader may compare the  $d$  values we use in our experiments with the dimensions of the maps shown in Tab. A1.

**Table 3:** Performance of the d-TEA with various triangular meshes for various values of  $d$  (summary).

mesh type	$d = \infty$			$d = 128$			$d = 64$			$d = 32$			$d = 16$			$d = 8$			$d = 4$			$d = 2$		
	$\bar{t}_c$	$\% \bar{\eta}_T$	$\% \bar{t}_q$	$\bar{t}_c$	$\% \bar{\eta}_T$	$\% \bar{t}_q$	$\bar{t}_c$	$\% \bar{\eta}_T$	$\% \bar{t}_q$	$\bar{t}_c$	$\% \bar{\eta}_T$	$\% \bar{t}_q$	$\bar{t}_c$	$\% \bar{\eta}_T$	$\% \bar{t}_q$	$\bar{t}_c$	$\% \bar{\eta}_T$	$\% \bar{t}_q$	$\bar{t}_c$	$\% \bar{\eta}_T$	$\% \bar{t}_q$	$\bar{t}_c$	$\% \bar{\eta}_T$	$\% \bar{t}_q$
CDT <sup>1</sup>	0	177.5*	8.44*	0	155.8	10.14	0	111.4	7.85	0	59.6	4.90	0	26.1	2.74	0	10.6	1.56	0	4.5	0.99	0	2.1	0.73
MinLT	6*	-8.1*	-12.1*	6	-7.8	-10.6	6	-6.9	-8.6	6	-6.4	-5.9	6	-6.9	-2.4	6	-9.3	0.2	6	-12.3	1.8	6	-14.3	3.1
MinVT-2	212*	-13.9*	-15.9*	212	-12.4	-12.9	212	-8.9	-8.8	212	-5.2	-2.9	212	-2.2	3.4	212	-0.7	7.2	212	-0.4	8.8	212	0.0	9.0
MinVT-4	96*	-12.3*	-14.7*	96	-11.0	-12.1	96	-8.0	-8.4	96	-4.8	-3.0	96	-2.3	2.8	96	-1.4	6.1	96	-1.3	7.7	96	-0.9	8.2
MinVT-8	44*	-8.2*	-12.3*	44	-7.2	-10.1	44	-4.8	-7.0	44	-2.3	-1.8	44	-0.3	3.3	44	0.7	6.8	44	2.0	9.1	44	3.7	9.7
MinVTO-2	23*	-13.1*	-15.3*	23	-11.9	-12.7	23	-9.2	-9.4	23	-6.3	-4.4	23	-4.2	1.0	23	-3.8	4.5	23	-4.4	6.2	23	-4.7	6.8
MinVTO-4	13*	-11.5*	-14.1*	13	-10.5	-11.9	13	-8.1	-8.8	13	-5.6	-4.3	13	-4.0	0.6	13	-4.1	3.9	13	-4.8	5.5	13	-4.9	6.1
MinVTO-8	9*	-7.6*	-11.8*	9	-6.8	-9.8	9	-4.8	-7.1	9	-2.9	-2.9	9	-1.6	1.6	9	-1.3	4.8	9	-0.7	6.7	9	0.6	7.7
d-MinVT-2	-	-	-	189	-12.7	-13.1	131	-10.4	-10.5	71	-8.8	-6.6	35	-8.8	-2.9	20	-10.7	-0.0	15	-13.2	2.4	13	-15.1	2.6
d-MinVT-4	-	-	-	93	-11.2	-12.3	66	-9.2	-9.7	39	-8.0	-6.3	22	-8.2	-2.7	14	-10.2	0.5	11	-12.8	2.2	10	-14.3	2.9
d-MinVT-8	-	-	-	47	-7.5	-10.1	35	-6.1	-7.8	23	-5.7	-4.9	15	-6.6	-1.6	11	-8.6	1.1	9	-10.5	3.9	9	-12.0	4.2
d-MinVTO-2	-	-	-	27	-12.1	-13.0	24	-10.0	-10.0	18	-8.6	-6.6	13	-8.6	-2.6	10	-10.5	0.2	9	-13.0	2.9	8	-14.9	3.0
d-MinVTO-4	-	-	-	16	-10.6	-11.9	15	-8.9	-9.6	12	-7.8	-6.0	10	-8.0	-2.5	8	-10.0	0.5	8	-12.6	2.4	7	-14.1	3.2
d-MinVTO-8	-	-	-	12	-7.0	-9.7	11	-5.9	-7.8	10	-5.5	-5.0	9	-6.4	-1.4	8	-8.5	1.1	7	-10.3	3.8	7	-11.9	3.7

*Legend:*  $d$  is the visibility range. Otherwise, the legend is the same as in Tab. 2, but all the values are averaged over all test maps.

*Units:*  $d$  is in meters;  $\bar{t}_c$  is in seconds;  $\% \bar{\eta}_T$ , and  $\% \bar{t}_q$  are in percents except for CDT (see footnote<sup>1</sup>).

*Note:* The values marked with \* also appear at the bottom of Tab. 2 (avg row).

<sup>1</sup> The values in  $\% \bar{\eta}_T$  and  $\% \bar{t}_q$  columns are absolute for the CDT:  $\bar{\eta}_T$  is a mean count,  $\bar{t}_q$  is in microseconds. The same values are relative percentage gaps w.r.t. CDT for the other mesh types.



Furthermore, according to the expansions, the gap between d-MinVT-2 and MinLT is getting lower with lower visibility ranges. This is caused by the fact that their weights are getting more (approximately) proportional. Note that as we lower the visibility range, the area visible from a segment depends more proportionally on the segment's length.

The last observation we want to point out is the increasing inconsistency between the numbers of expansions and query times for decreasing  $d$ . Starting with  $d = 8$ , the CDT is, in fact, the best-performing mesh according to the measured query time. This is contrary to what the expansions tell us. We explain this the following way. Unlike the TEA, the d-TEA outputs different (temporary) regions for the same queries and various meshes. The circle intersection only then unifies these regions to be the same. The temporary regions' difference is due to d-TEA expanding until full edges are outside the visibility range, which depends on how the edges are organized. Different temporary regions affect the circle intersection computation times, which may outweigh the effect of lowering the number of expansions. Therefore, this whole observation suggests that when the visibility range is considerably limited, the CDT might be closer to the actual optimal mesh than the proposed mesh minimizing the number of expansions. But what is the actual optimal mesh, then? Probably the one that minimizes the combination of the number of expansions and the laboriousness of the circle intersection. Formalizing this idea is an interesting open question.

## 6 Conclusion

In this paper and its proceedings' predecessor [4], we addressed the problem of improving the query performance of the TEA [3] for computing visibility regions with only one variable component—the instance of the triangular mesh, i.e., the preprocessing structure. Based on the equations in Sec. 3, experiments on the 11 maps from various sources performed in [4], and more thorough experiments on the challenging 25 maps [6] from the Iron Harvest videogame achieved in this paper, we can now answer the following scientific and practical questions.

- *Does the choice of mesh influence the query performance of the algorithm?*—Yes. We measured the mean query time of 1 million identical queries for many different meshes. The largest obtained gap between two meshes was 116%; the better of the two had  $13.7 \mu s$ , and the worse  $29.7 \mu s$ .
- *Can some other more exact metric be used to access the mesh performance?*—Yes. The number of triangle edge expansions is approximately proportional to the measured computational time.
- *Is there an optimal mesh?*—The optimal mesh can be defined as in Eq. (7) based on the expected number of edge expansions assuming the query points are drawn from a known probability distribution. The proposed MinVT defined in Eq. (13) well approximates the optimal mesh, assuming

all possible queries are equally likely and the map resembles a real-world environment.

- *Is there a way to construct the optimal mesh?*—The problem of finding the optimal mesh is NP-hard. However, in Sec. 4 we propose a heuristic algorithm that provides good approximations; we include a guide to tuning its parameters and describe the implementation, which is publicly available.
- *What is the expected improvement and what are the costs?*—The following values are the average results from our experiments. The MinVT shortens the mean query times by about 12-16% for the cost of 9-212 s of preprocessing, depending on the parameters, compared to the reference CDT. The MinLT, i.e., the mesh minimizing edge lengths, also performs better than CDT by 12% and takes 6 s to construct. The CDT, on the other hand, takes effectively zero time to construct.
- *What if the visibility range is limited?*—The d-TEA, which is part of our implementation, can handle it efficiently. Depending on the range, the best-performing mesh is either d-MinVT or CDT. The CDT is better for small ranges because it outputs temporary regions which are easier to intersect with a circle. The optimal d-TEA mesh would need to include this operation in the optimizing criterion.

In conclusion, our approach can be used to boost offline applications that require computing millions of queries in complex real-world environments, where long preprocessing time is not an issue. Otherwise, the CDT is the best choice for its simplicity and fast construction. The ideas presented in this paper may inspire attempts to improve some other mesh algorithms similarly. Furthermore, our implementation may serve the community.

## Acknowledgments

This work was supported by the European Regional Development Fund under the project Robotics for Industry 4.0 (reg. no. CZ.02.1.01/0.0/0.0/15003/000 0470) and by the Grant Agency of the Czech Technical University in Prague, grant No. SGS21/185/OH K3/3T/37.

## Declarations

**Conflict of interest** On behalf of all authors, the corresponding author states that there is no conflict of interest.

## Appendix A Map Properties

In this paper, we use as the benchmark instances the 35 polygonal maps from [6], which are based on the videogame Iron Harvest developed by KING Art Games. The instances were originally created for the pathfinding community, but they are also ideal for benchmarking algorithms for computing

**Table A1:** Properties of the polygonal maps.

Full name	Abbrev.	$n$ [1]	$h$ [1]	$x$ [m]	$y$ [m]	$a$ [m <sup>2</sup> ]	Used in tuning?
scene_mp_2p_01	2p1	3219	263	200.00	210.00	35095.74	
scene_mp_2p_02	2p2	2318	165	270.00	270.00	54034.51	
scene_mp_2p_03	2p3	3627	199	330.00	311.35	59301.76	✓
scene_mp_2p_04	2p4	1937	63	240.00	310.00	52910.41	
scene_mp_4p_01	4p1	4173	407	320.00	320.00	75593.44	
scene_mp_4p_02	4p2	6180	376	380.00	525.00	110844.68	✓
scene_mp_4p_03	4p3	7495	632	400.00	410.00	98462.60	
scene_mp_6p_01	6p1	5068	376	368.42	498.36	122027.57	
scene_mp_6p_02	6p2	5366	297	399.57	440.00	130703.25	✓
scene_mp_6p_03	6p3	4702	287	500.00	500.00	152452.47	
scene_sp_cha_01	ch1	2425	174	230.00	280.00	46392.01	✓
scene_sp_cha_02	ch2	3436	254	335.00	570.00	176524.94	
scene_sp_cha_03	ch3	5370	454	400.00	430.00	99961.38	
scene_sp_cha_04	ch4	6616	623	440.00	440.00	124769.37	
scene_sp_endmaps	end	8068	675	565.00	770.00	361157.48	
scene_sp_pol_01	p11	1055	63	323.10	132.93	12888.24	
scene_sp_pol_02	p12	5319	336	470.00	515.00	98318.65	
scene_sp_pol_03	p13	6828	558	420.00	510.00	127591.60	
scene_sp_pol_04	p14	6231	479	350.00	340.00	73878.85	✓
scene_sp_pol_05	p15	3966	339	515.00	394.60	85649.98	
scene_sp_pol_06	p16	8320	679	470.00	480.00	157202.02	✓
scene_sp_rus_01	rs1	3125	276	330.65	223.97	33855.12	
scene_sp_rus_02	rs2	2724	167	304.60	307.48	34607.91	
scene_sp_rus_03	rs3	4878	372	450.00	430.00	70253.34	✓
scene_sp_rus_04	rs4	5628	360	338.27	500.00	104914.01	
scene_sp_rus_05	rs5	6018	367	404.41	418.64	85143.08	✓
scene_sp_rus_06	rs6	7958	598	545.00	455.00	112490.37	
scene_sp_rus_07	rs7	3599	206	460.00	380.00	86095.22	
scene_sp_sax_01	sx1	2413	163	380.00	485.00	79226.77	
scene_sp_sax_02	sx2	7038	368	403.48	636.57	118046.67	✓
scene_sp_sax_03	sx3	6708	368	510.00	585.00	153676.22	
scene_sp_sax_04	sx4	6925	431	585.00	675.00	142835.44	
scene_sp_sax_05	sx5	1954	65	445.00	420.00	86942.15	
scene_sp_sax_06	sx6	4403	269	405.00	465.00	97323.07	
scene_sp_sax_07	sx7	4151	348	310.00	340.00	69575.62	✓

*Legend:*  $n$  is the number of map vertices (i.e., corners);  $h$  is the number of holes (i.e., obstacles);  $x$  and  $y$  are the width and height of the map, respectively;  $a$  is the map's area. The checkmark ✓ means that the instance was used for tuning the parameters of our approach in Sec. 5.2 and excluded from the main experiments in Sec. 5.3-5.4.

visibility regions. The authors provide three types of representations: polygonal, mesh, and grid. Since our paper is about creating meshes from polygons, we have chosen the polygonal representation. To get the single polygon with holes that our algorithms require, we select only the largest polygon from the provided representation and include all holes it contains with it.

The resulting maps are considerably complex polygons defined by thousands of vertices and dozens to hundreds of holes, mostly spanning about  $400 \times 400$  meters. Note that the choice of unit (meters) is arbitrary, but it

must correspond to some of our parameters, e.g.,  $d$  and  $d_{\text{samp}}$ . Tab. A1 shows detailed properties of all the maps.

## References

- [1] Davis, L.S., Benedikt, M.L.: Computational models of space: Isovists and isovist fields. *Computer Graphics and Image Processing* **11**(1), 49–72 (1979)
- [2] Asano, T.: An efficient algorithm for finding the visibility polygon for a polygonal region with holes. *IEICE Transactions* **68**(9), 557–559 (1985)
- [3] Bungiu, F., Hemmer, M., Hershberger, J., Huang, K., Kröller, A.: Efficient Computation of Visibility Polygons. *arXiv:1403.3905* (2014)
- [4] Mikula, J., Kulich, M.: Triangular Expansion Revisited: Which Triangulation Is The Best? In: *Proceedings of the 19th International Conference on Informatics in Control, Automation and Robotics*, pp. 313–319 (2022)
- [5] Shewchuk, J.R.: Delaunay refinement algorithms for triangular mesh generation. *Computational Geometry* **22**(1), 21–74 (2002)
- [6] Harabor, D., Hechenberger, R., Jahn, T.: Benchmarks for pathfinding search: Iron harvest. In: *Proceedings of the International Symposium on Combinatorial Search*, vol. 15, pp. 218–222 (2022)
- [7] Joe, B., Simpson, R.B.: Corrections to Lee’s Visibility Polygon Algorithm. *BIT* **27**(4), 458–473 (1987)
- [8] Heffernan, P.J., Mitchell, J.S.B.: An Optimal Algorithm for Computing Visibility in the Plane. *SIAM Journal on Computing* **24**(1), 184–201 (1995)
- [9] Zarei, A., Ghodsi, M.: Query point visibility computation in polygons with holes. *Computational Geometry* **39**(2), 78–90 (2008)
- [10] Inkulu, R., Kapoor, S.: Visibility queries in a polygonal region. *Computational Geometry* **42**(9), 852–864 (2009)
- [11] Chen, D.Z., Wang, H.: Visibility and ray shooting queries in polygonal domains. *Computational Geometry* **48**(2), 31–41 (2015)
- [12] Kulich, M., Preučil, L., Bront, J.J.M.: Single robot search for a stationary object in an unknown environment. In: *Proceedings of 2014 IEEE International Conference on Robotics and Automation*, pp. 5830–5835 (2014)

- [13] Kulich, M., Miranda Bront, J.J., Přeučil, L.: A meta-heuristic based goal-selection strategy for mobile robot search in an unknown environment. *Computers & Operations Research* **84** (2017)
- [14] Kulich, M., Kubalík, J., Přeučil, L.: An Integrated Approach to Goal Selection in Mobile Robot Exploration. *Sensors* **19**(6) (2019)
- [15] O'Rourke, J.: *Art Gallery Theorems and Algorithms*. Oxford University Press, Inc. (1987)
- [16] Ntafos, S.: Watchman routes under limited visibility. *Computational Geometry: Theory and Applications* **1**(3), 149–170 (1992)
- [17] Guibas, L.J., Latombe, J.-C., LaValle, S.M., Lin, D., Motwani, R.: Visibility-based pursuit-evasion in a polygonal environment. In: *Workshop on Algorithms and Data Structures*, pp. 17–30 (1997). Springer
- [18] Mikula, J., Kulich, M.: Towards a Continuous Solution of the d-Visibility Watchman Route Problem in a Polygon With Holes. *IEEE Robotics and Automation Letters* **7**(3), 5934–5941 (2022)
- [19] CGAL: Computational Geometry Algorithms Library. <https://www.cgal.org/>
- [20] Arkin, E.M., Efrat, A., Knauer, C., Mitchell, J.S., Polishchuk, V., Rote, G., Schlipf, L., Talvitie, T.: Shortest path to a segment and quickest visibility queries. *Journal of Computational Geometry* **7**(2), 77–100 (2016)
- [21] Cui, M., Harabor, D.D., Grastien, A.: Compromise-free Pathfinding on a Navigation Mesh. In: *Proceedings of the Twenty-Sixth International Joint Conference on Artificial Intelligence, IJCAI-17*, pp. 496–502 (2017)
- [22] Shen, B., Cheema, M.A., Harabor, D., Stuckey, P.J.: Euclidean Pathfinding with Compressed Path Databases. In: *Proceedings of the Twenty-Ninth International Joint Conference on Artificial Intelligence, IJCAI-20*, pp. 4229–4235 (2020)
- [23] Keynes, J.M.: The Principle of Indifference. In: *A Treatise on Probability* vol. 4, pp. 41–64. Macmillan and Co., London (1921). Chap. IV
- [24] Grantson, M., Borgelt, C., Levkopoulos, C.: Fixed Parameter Algorithms for the Minimum Weight Triangulation Problem. *International Journal of Computational Geometry & Applications* **18**(03), 185–220 (2008)
- [25] Mulzer, W., Rote, G.: Minimum-Weight Triangulation is NP-Hard. *Journal of the ACM (JACM)* **55**(2), 1–29 (2008)

- [26] Shewchuk, J.R.: Adaptive Precision Floating-Point Arithmetic and Fast Robust Geometric Predicates. *Discrete & Computational Geometry* **18**(3), 305–363 (1997)
- [27] Fišer, D., Faigl, J., Kulich, M.: Growing neural gas efficiently. *Neurocomputing* **104**, 72–82 (2013)
- [28] Edahiro, M., Kokubo, I., Asano, T.: A new point-location algorithm and its practical efficiency: comparison with existing algorithms. *ACM Transactions on Graphics (TOG)* **3**(2), 86–109 (1984)
- [29] Shewchuk, J.R.: Triangle: Engineering a 2D Quality Mesh Generator and Delaunay Triangulator. *Applied Computational Geometry Towards Geometric Engineering* **1148**, 203–222 (1996)